DOI: 10.48011/asba.v2i1.1427

Parameters Design and Performance Analysis for Grid-tied VSG-Controlled Converters

Thiago F. do Nascimento * **Luciano S. Barros** ** **Flavio B. Costa** *

* *Federal University of Rio Grande do Norte (UFRN), (e-mail: figueiredo.21@hotmail.com, flaviocosta@ect.ufrn.br)*
** *Federal University of Paraiba (UFPB), (e-mail: lsalesbarros@ci.ufpb.br)*

Abstract: The high penetration of distributed generation (DG) systems based on renewable energy sources (RES) requires the development of control techniques for improving the support to the grid frequency and voltage. Among the solutions proposed in the literature, the virtual synchronous generator (VSG) concept has proven to be an attractive solution to interconnect DG units to the power grid. However, the dynamic behavior of the VSG has not yet been discussed for cases in which line impedance parameters varies in relation to their rated values. To evaluate this issue, a dynamic model of VSG power flow has been derived and its dynamic characteristics discussed in this work. Based on this model, parameters for VSG controllers are designed by using root-locus method (RLM) in order to realize desired dynamic performance. Then, the VSG dynamic performance under line impedance variation effect is assessed. Finally, simulation results demonstrate the effectiveness of the theoretical analysis and parameters design method.

Keywords: Distributed generation, renewable energy sources, root locus method, virtual synchronous generator.

1. INTRODUCTION

The DG units are grid-interfaced by power converters and can operate as controlled current sources or controlled voltage sources, as well as providing grid support (Rocabert et al., 2012). Most of the DG grid-tied systems act as controlled current sources (Blaabjerg et al., 2006), however, this control method is acceptable only in power systems with RES low penetration level, in which any power fluctuation is compensated by the conventional synchronous generators (SG) for achieving the system power balance (Zhong, 2016). In power systems with RES high penetration level, the stability margin imposed by the conventional GSs tends to decrease due to the inherent intermittence of the renewable sources and the lack of inertia and damping of the DG units (Azmy and Erlich, 2005). In this scenario, DG units operating as controlled voltage sources could provide higher performance to the system and actively taking part in the grid power regulation, as the conventional SGs (Shuai et al., 2016), since they had the ability to control the power flow delivered to the grid.

Some methods for improving the power flow control have been proposed. Among them, the VSG has gained more attention due to its operation similarity with conventional SG (Zhong, 2016). This method employs the droop mechanism and inertial characteristic inherent to conventional SGs in order to regulate DG power flow. As a result, the DG grid-tied converter has the ability of providing grid support by regulating its active and reactive power according to the output frequency and voltage for achieving a suitable power balance. In the recent years, various methods for VSG implementation have been discussed (Mo et al., 2017). Due to the VSG is implemented in software, its parameters can be designed to achieve the desired dynamic performance and stability requirements. In general, the model applied to the VSG power flow describes only its behavior in steady state neglecting the transient behavior related to line impedance variations (Zhang et al., 2010). Therefore, more rigorous mathematical models are needed to realize desired dynamic performance through design of control parameters.

In the literature, some work focus on the small signal modeling and parameters design for VSG approach, as described below. The RLM is employed in Du et al. (2013) and Song et al. (2018), but the transient characteristics related to the VSG power flow are not considered in its dynamic models, thus the designed parameters may not be appropriate being needed further adjustments to obtain the desired results. In Guerrero et al. (2004), Guerrero et al. (2007), and Wu et al. (2016), the closed-loop transfer function of power flow control was derived for analysis and parameters design by using Frequency Response Design Method (FRDM), however, the transient effect related to the line impedance is not also considered. Thus, in Guerrero et al. (2004) and Guerrero et al. (2007), the control parameters of active and reactive power were partially tuned by trial-and-error, while in Wu et al. (2016), the power reference tracking performance without considering the required performance to system transient response is mainly presented. Besides, when DG units

are operating in grid-connected mode, it is essential to evaluate the control performance under line impedance variation conditions and analyze the effect on the power flow dynamic response and stability. However, these issues have not yet been well discussed.

In this paper, the dynamic model obtained for VSG power flow includes transient characteristics which depends on the line impedance. Thus, power control parameters can be designed accurately. The droop gain values are designed following the proper standards, while the VSG parameters values are designed by using RLM. Besides, the relationship between the power dynamic response and line impedance variation is discussed. Finally, simulation results verify the theoretical analysis and effectiveness of the parameters design method.

This paper is organized as follows. Section II presents the system description and derives its small-signal model. The control scheme and design criteria applied for the VSG Controllers are presented in detail in Section III. The simulation results and performance analysis are presented in Section IV, while Section V concludes this paper.

2. SYSTEM DESCRIPTION AND MODELING

Fig. 1 shows a typical topology and control scheme of the Grid-tied converter. The VSG algorithm is implemented with a three-phase voltage-source inverter (VSI) connected to point of common coupling (PCC) through a LC-filter. The DC voltage source represents the primary source of the Grid-tied converter (i.e., photovoltaic or wind power system). The LC-filter consists of the inductor L_i and the capacitor C_f, wherein r_i is the intrinsic resistance of the filter inductor. The power grid is represented by a three-phase voltage source interconnected to PCC through an equivalent line impedance composed by series connected inductors L_g and resistors R_g.

2.1 Grid-Tied Voltage Source Converter Modeling

The grid-tied converter model operating as a controllable voltage source corresponds to the LC-filter dynamic model. Thus, the transfer functions for grid-tied current and voltage control loops are obtained by Kirchhoff laws applied to LC-filter, Fig. 1. Therefore, the transfer function that describes the VSI output currents is defined as:

$$G_I(s) = \frac{I^e_{odq}(s)}{E'^e_{dq}(s)} = \frac{1}{L_i s + r_i}, \tag{1}$$

where $E'^e_{dq}(s) = E^e_{dq}(s) - V^e_{odq}(s)$, superscript e refers to the synchronous reference frame. By using similar procedure, the transfer function that describes the PCC voltage is:

$$G_V(s) = \frac{V^e_{odq}(s)}{I^e_{cdq}(s)} = \frac{1}{C_f s}, \tag{2}$$

where $I^e_{cdq}(s) = I^e_{odq}(s) - I^e_{gdq}(s)$. The terms $V^e_{odq}(s)$ and $I^e_{gdq}(s)$ present in these models, as well as the terms corresponding to coupling between the dq variables are considered disturbances to be compensated by the voltage and current controllers (see Fig. 1).

2.2 VSG Power Flow Modeling

For a predominantly inductive line impedance, it is possible to obtain a direct relationship between active power and load angle, as well as between reactive power and voltage magnitude (Rocabert et al., 2012). Based on this idea, the modeling applied to VSG power flow, which describes the relations P_o/δ and Q_o/V_o, is based on the methodology developed in Zhang et al. (2010). Therefore, considering the three-phase symmetrical system, the active (P_o) and reactive (Q_o) power provided to power grid are calculated according to the instantaneous power theory (Akagi et al., 2017), and can be given by:

$$P_o = v^e_{od} i^e_{gd} + v^e_{oq} i^e_{gq}, \tag{3}$$

$$Q_o = v^e_{oq} i^e_{gd} - v^e_{od} i^e_{gq}, \tag{4}$$

where v^e_{od}, v^e_{oq}, i^e_{gd} and i^e_{gq} are the PCC voltage and VSG output currents, respectively, in the synchronous reference frame. Assuming that any variable x in these equations is equal to operating point value x_n added to a small ac variation $\hat{x}$, (3) and (4) can be rewritten as:

$$\hat{P}_o(s) = \begin{bmatrix} I^e_{gdn} \\ I^e_{gqn} \end{bmatrix}^T \cdot \begin{bmatrix} \hat{V}^e_{od}(s) \\ \hat{V}^e_{oq}(s) \end{bmatrix} + \begin{bmatrix} V^e_{odn} \\ V^e_{oqn} \end{bmatrix}^T \cdot \begin{bmatrix} \hat{I}^e_{gd}(s) \\ \hat{I}^e_{gq}(s) \end{bmatrix}, \tag{5}$$

$$\hat{Q}_o(s) = \begin{bmatrix} I^e_{gdn} \\ -I^e_{gqn} \end{bmatrix}^T \cdot \begin{bmatrix} \hat{V}^e_{oq}(s) \\ \hat{V}^e_{od}(s) \end{bmatrix} + \begin{bmatrix} V^e_{odn} \\ V^e_{oqn} \end{bmatrix}^T \cdot \begin{bmatrix} -\hat{I}^e_{gq}(s) \\ \hat{I}^e_{gd}(s) \end{bmatrix}, \tag{6}$$

where the dc terms and terms formed by the product of ac quantities were neglected, and then Laplace transformation was applied.

Kirchhoff voltage law applied to three-phase system represented by the PCC connected to the mains through a line impedance (see Fig. 1) provides the following dynamic equation in the dq synchronous reference frame:

$$v^e_{odq} = R_g i^e_{gdq} + L_g \frac{di^e_{gdq}}{dt} + \omega_g L_g \begin{bmatrix} 0 & -1 \\ 1 & 0 \end{bmatrix} i^e_{gdq} + v^e_{gdq}, \tag{7}$$

which can be rewritten in terms of dq components, such as:

$$L_g \frac{di^e_{gd}}{dt} = V_o\sqrt{3}\cos(\delta) - V_g\sqrt{3} - R_g i^e_{gd} + \omega_g L_g i^e_{gq}, \tag{8}$$

$$L_g \frac{di^e_{gq}}{dt} = V_o\sqrt{3}\sin(\delta) - R_g i^e_{gq} - \omega_g L_g i^e_{gd}, \tag{9}$$

where ω_g is grid angular frequency. Considering PCC voltage magnitude constant, i.e., $V_o = V_{on}$, and assuming the load angle varies around the operating point as $\delta = \delta_n + \hat{\delta}$, (8) and (9) can be linearized as:

$$L_g \frac{d\hat{i}^e_{gd}}{dt} = -V_{on}\sqrt{3}\sin(\delta_n)\hat{\delta} - R_g \hat{i}^e_{gd} + \omega_g L_g \hat{i}^e_{gq}, \tag{10}$$

$$L_g \frac{d\hat{i}^e_{gq}}{dt} = V_{on}\sqrt{3}\cos(\delta_n)\hat{\delta} - R_g \hat{i}^e_{gq} - \omega_g L_g \hat{i}^e_{gd}, \tag{11}$$

where again the dc terms and terms formed by the product of ac quantities were neglected. Thus, applying Laplace transformation in (10) and (11) results in the following expression:

$$\begin{cases} \hat{I}^e_{gd}(s) = V_{on}\sqrt{3}\left[\dfrac{\omega_g L_g cos(\delta_n) - (sL_g + R_g)sin(\delta_n)}{(sL_g + R_g)^2 + (\omega_g L_g)^2}\right]\hat{\delta}(s), \\ \hat{I}^e_{gq}(s) = V_{on}\sqrt{3}\left[\dfrac{\omega_g L_g sin(\delta_n) + (sL_g + R_g)cos(\delta_n)}{(sL_g + R_g)^2 + (\omega_g L_g)^2}\right]\hat{\delta}(s). \end{cases} \tag{12}$$

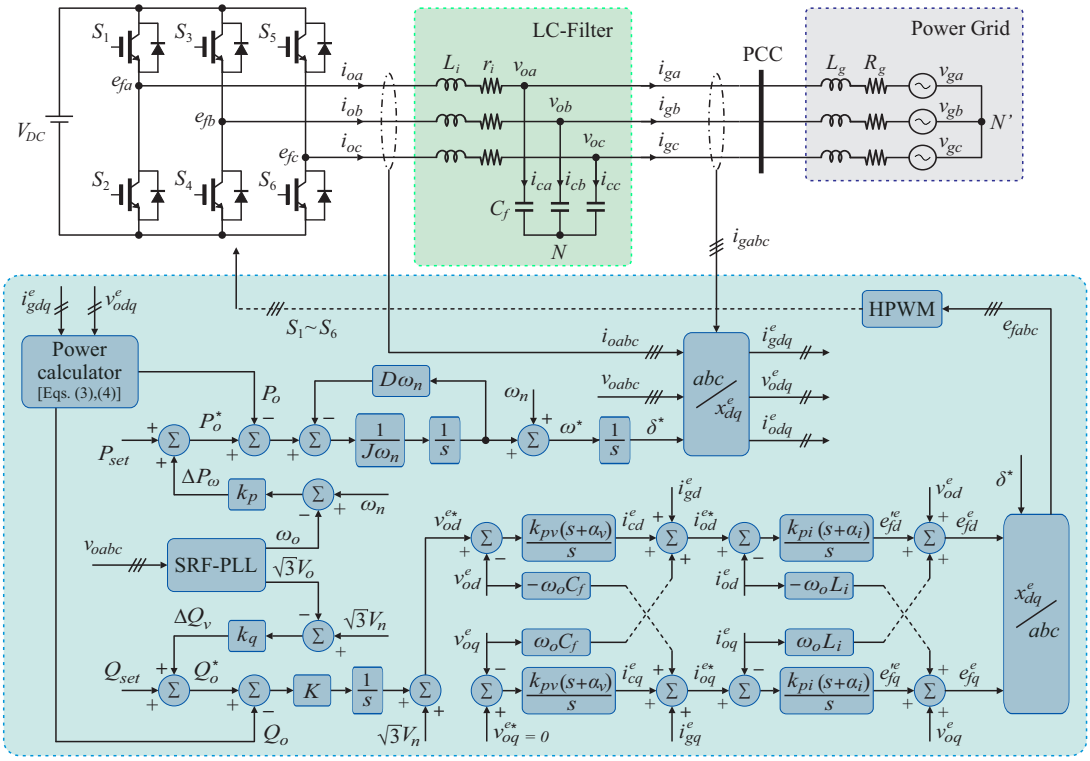

Figure 1. Block diagram of the Grid-tied converter with its control strategy.

The terms $\hat{V}^e_{od}(s)$ and $\hat{V}^e_{oq}(s)$ can be obtained linearizing (7) around the operating point, and then applying Laplace transformation, as follows:

$$\begin{cases} \hat{V}^e_{od}(s) = (sL_g + R_g)\hat{I}^e_{gd}(s) - \omega_g L_g \hat{I}^e_{gq}(s), \\ \hat{V}^e_{oq}(s) = (sL_g + R_g)\hat{I}^e_{gq}(s) + \omega_g L_g \hat{I}^e_{gd}(s). \end{cases} \tag{13}$$

The dq components of the PCC voltage at the operating point can be expressed as:

$$\begin{cases} V^e_{odn} = V_{on}\sqrt{3}cos(\delta_n), \\ V^e_{oqn} = V_{on}\sqrt{3}sin(\delta_n). \end{cases} \tag{14}$$

Moreover, current provided to power grid in terms of dq complex variables can be expressed by:

$$I^e_{gdn} + jI^e_{gqn} = \frac{(V^e_{odn} + jV^e_{oqn}) - (V^e_{gdn} + jV^e_{gqn})}{R_g + j\omega_g L_g}, \tag{15}$$

where $V^e_{gdn} = V_{gn}\sqrt{3}$, and $V^e_{gqn} = 0$. Thus, (15) can be rewritten in terms dq components, such as:

$$\begin{cases} I^e_{gdn} = \dfrac{R_g\left(V^e_{odn} - V^e_{gdn}\right) + \omega_g L_g V^e_{oqn}}{R_g^2 + (\omega_g L_g)^2}, \\ I^e_{gqn} = \dfrac{R_g V^e_{oqn} - \omega_g L_g\left(V^e_{odn} - V^e_{gdn}\right)}{R_g^2 + (\omega_g L_g)^2}. \end{cases} \tag{16}$$

By substituting (12), (13), (14) and (16) into (5), and assuming small values applied to δ_n, the linearized dynamic model for VSG active power provided to power grid can be given by:

$$G_P(s) = \frac{\hat{P}_o(s)}{\hat{\delta}(s)} = \frac{h_p}{s^2 + \frac{2R_g}{L_g}s + \frac{R_g^2 + (\omega_g L_g)^2}{L_g^2}} \tag{17}$$

in which

$$h_p = \frac{3V_{on}V_{gn}}{L_g^2}(R_g sin(\delta_n) + \omega_g L_g cos(\delta_n)). \tag{18}$$

The transfer function represented by (17) is the small-signal ac model which denotes the dynamics relationship between active power ($\hat{P}_o$) and load angle variation ($\hat{\delta}$).

By using similar procedure, the linearized dynamic model for VSG reactive power delivered to power grid can be derived considering load angle constant, i.e., $\delta = \delta_n$, and assuming $V_o = V_{on} + \hat{V}_o$. Thus, linearizing again (8) and (9) around the operating point, and then applying Laplace transformation results in the expression:

$$\begin{cases} \hat{I}^e_{gd}(s) = \sqrt{3}\left[\dfrac{\omega_g L_g sin(\delta_n) + (sL_g + R_g)cos(\delta_n)}{(sL_g + R_g)^2 + (\omega_g L_g)^2}\right]\hat{V}_o(s), \\ \hat{I}^e_{gq}(s) = \sqrt{3}\left[\dfrac{-\omega_g L_g cos(\delta_n) + (sL_g + R_g)sin(\delta_n)}{(sL_g + R_g)^2 + (\omega_g L_g)^2}\right]\hat{V}_o(s). \end{cases} \tag{19}$$

By substituting (13), (14), (16) and (19) into (6), and assuming small values to δ_n, results in the following expression:

$$G_Q(s) = \frac{\hat{Q}_o(s)}{\hat{V}_o(s)} = \frac{h_q}{s^2 + \frac{2R_g}{L_g}s + \frac{R_g^2 + (\omega_g L_g)^2}{L_g^2}} \tag{20}$$

in which

$$h_q = \frac{3}{L_g^2}(\omega_g L_g(2V_{on} + V_{gn}cos(\delta_n)) - R_g V_{gn} sin(\delta_n)). \tag{21}$$

The transfer function represented by (20) is the small-signal ac model which correlates the VSG reactive power variation ($\hat{Q}_o$) with PCC voltage variation ($\hat{V}_o$).

2.3 VSG Power Flow Dynamic Analysis

The models described by (17) and (20) represent the transfer function typical second-order systems with identical poles and calculated as:

$$s_{1,2} = -\frac{R_g}{L_g} \pm j\omega_g. \tag{22}$$

The poles are always negative, indicating a VSG power flow stable for a wide range of adjustment. Besides, pole locations vary as a function of the line impedance parameters and grid angular frequency. Thus, the natural oscillation frequency ω_{PQ} and damping ratio ξ_{PQ} related to these models are calculated as:

$$\omega_{PQ} = \frac{\sqrt{R_g^2 + (\omega_g L_g)^2}}{L_g}, \tag{23}$$

$$\xi_{PQ} = \frac{R_g}{\sqrt{R_g^2 + (\omega_g L_g)^2}}. \tag{24}$$

Fig. 2 shows the natural oscillation frequency and damping ratio for different X/R ratio values. When X/R ratio increases from 1.25 to 5.1, the natural oscillation frequency decreases from 483 to 385 rad/s, while the damping ratio decreases from 0.62 to 0.2, approximately, which represents a degradation of dynamic performance.

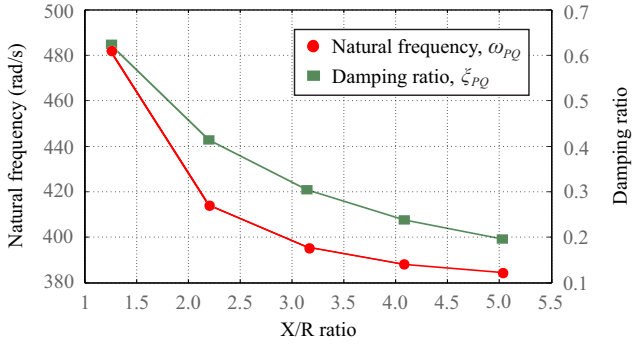

Figure 2. Natural frequency and damping ratio when the X/R ratio varies.

Fig. 3 shows the root locus plots for models $G_P(s)$ and $G_Q(s)$ using parameters described in Table 1 and different X/R ratio values. As X/R ratio is increasing the closed-loop poles are closer to the origin, system damping and natural oscillation frequency will be decreased and the overshoot will be increased, resulting in a more oscillatory dynamic response. On the other hand, with the decrease of X/R ratio, the closed-loop poles are furthest to the origin, system damping and natural oscillation frequency will be increased and the overshoot will be decreased, resulting in a more dampened dynamic response. Therefore, line impedance parameters variation has a lot of influence on the VSG power flow dynamic behavior, which in turn can degrade the active and reactive power controllers dynamic performance.

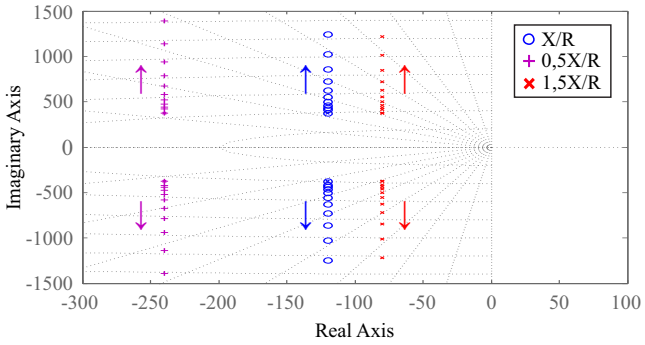

Figure 3. Root locus for $G_P(s)$ and $G_Q(s)$ with different X/R ratio values.

3. CONTROL SCHEME

Fig.1 presents the block diagram of the VSG control scheme which consists in three cascaded control loops. The outer loop regulates the VSG active and reactive power provided to the power grid. The VSG active power controller employs the emulation of the synchronous generator swing equation given by:

$$P_o^* - P_o - D\omega_n \frac{d\delta}{dt} = J\omega_n \frac{d^2\delta}{dt^2}, \tag{25}$$

where J represents the inertia moment, D the damping factor, ω_n the system nominal angular frequency and δ corresponds to the phase-angle difference between the PCC voltage and grid voltage. The VSG reactive power controller employs to the following dynamic equation:

$$Q_o^* - Q_o = \frac{1}{K}\frac{dV_o}{dt}, \tag{26}$$

where K represents a control integral gain. In this control scheme, the active power reference consists in $P_o^* = P_{set} + \Delta P_\omega$, in which $\Delta P_\omega = k_p(\omega_n - \omega_o)$. Similarly, the reactive power reference consists in $Q_o^* = Q_{set} + \Delta Q_v$, in which $\Delta Q_v = k_q(V_n - V_o)$. The gains k_p and k_q represent the droop coefficients. Also, the variables ω_n and V_n represent the system nominal frequency and voltage, respectively, while ω_o and V_o are estimations determined by a synchronous reference frame phase-locked loop (SRF-PLL). Therefore, since $\omega_o \approx \omega_g$ and $V_o \approx V_g$, the grid frequency and PCC voltage can be regulated by adjustment of the active and reactive power values provided to the power grid. The intermediate and inner loops regulate the PCC voltage and VSI output current, respectively, by using standard PI controllers. The reference frame employed in the voltage and current control loops follows the *dq* synchronous reference frame. The phase-angle δ^* applied to the orthogonal transformations between *abc* natural reference frame and *dq* synchronous reference frame is determined by the active power controller. The reference voltage v_{od}^{e*} for PCC voltage control is determined by the reactive power controller. Based on the reference voltages e_{fabc} delivered by the VSG current controller, HPWM strategy (Blasko, 1996) determines the drive signals of power switches $S1 - S6$.

3.1 Design Criteria applied for the VSG Controllers

This section describes the design criteria applied to controllers that implement the VSG control strategy. In this

paper, the design criterion used for determining the control gains employs the RLM. The implementation of the VSG grid-tied system presented in Fig. 1 employs the parameters described in Table 1.

Table 1. DG System Parameters

Parameters	Value
DC-Link voltage V_{DC}	900 V
Grid voltage V_g	127 V rms
Grid frequency ω_g	$2\pi 60$ rad/s
Grid impedance	$L_g = 5$ mH, $R_g = 0.6\ \Omega$
Rated power	10 kVA
Rated load angle δ_n	0.4 rad
Switching frequency	10 kHz
Filter inductor	$L_i = 3.5$ mH, $r_i = 0.1\ \Omega$
Filter capacitor C_f	10 μF

VSG Current Controller. The regulation of the VSG current employs standard PI controllers (see Fig. 1). Thus, considering the current model described by (1), the open-loop transfer function for VSG current control is given by:

$$T_I(s) = \frac{k_{pi}\,(s+\alpha_i)}{s\,(L_i s + r_i)}. \tag{27}$$

The PI gains were designed to meet the transient response requirements. Thus, assuming the settling time as design criterion, i.e., $T_{s2\%} = 1.5$ ms, the controller gain that address this design criterion is $k_{pi} = 9.4$. The controller zero was added without affecting the desired transient response. Therefore, a possible suitable zero can be found by using $\alpha_i = 9.57$, which results in a compensated system with two closed-loop real poles, one is found at $p_1 = -2700$, and a second pole at $p_2 = -9.51$. Fig. 4 shows the resulting root locus for VSG current control loop. The second closed-loop pole p_2 is close enough to the closed-loop zero to cause pole-zero cancellation, thus p_1 is closed-loop system dominant pole.

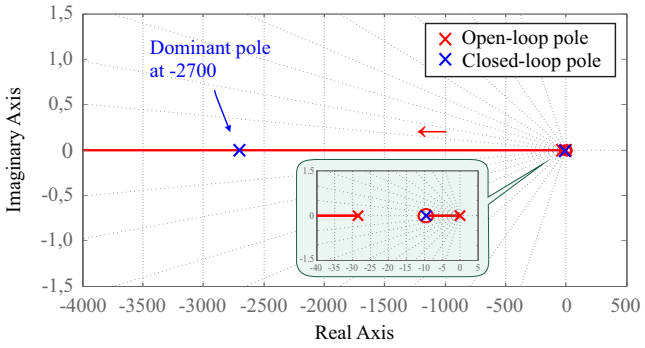

Figure 4. Root locus for VSG current control loop.

VSG Voltage Controller. The control strategy employs standard PI controllers for regulating the VSG output voltage (see Fig. 1), whose transfer function given by (2) describes its dynamic behavior. Thus, considering the inner current controller dynamics the open-loop transfer function for VSG voltage control is obtained as:

$$T_V(s) = \frac{k_{pi}k_{pv}\,(s+\alpha_i)\,(s+\alpha_v)}{L_i C_f s^2\,(s-p_1)\,(s-p_2)}. \tag{28}$$

For guaranteeing the suitable performance of the voltage control the performance requirements applied for determining the PI controller gains employs a percent overshoot (%OS) of 16, 5% and $T_{s2\%} = 1.5$ ms, which corresponds to $\xi_v = 0.5$ and $\omega_v = 2700$ rad/s. Thus, the controller gains that address these design requirements are $k_{pv} = 0.02714$ and $\alpha_v = 22.11$. Fig. 5 shows the resulting root locus for VSG voltage control loop. The closed-loop system has two complex dominant poles, and two real poles that are approximately canceled by the closed-loop zeros.

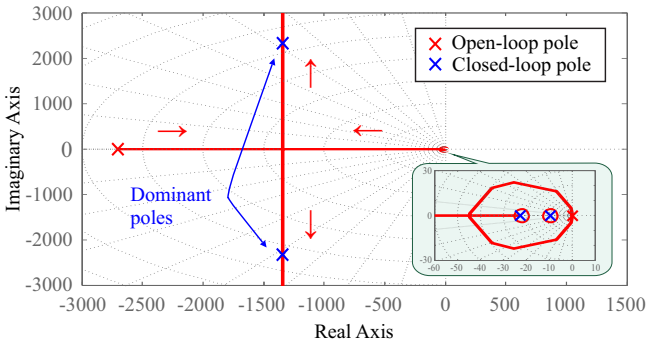

Figure 5. Root locus for VSG voltage control loop.

VSG Active Power Controller. According to block diagram of the Fig. 1 and considering $\omega_o \approx \omega^*$, the transfer function of the controller that regulate the VSG active power can be expressed as:

$$R_P(s) = \frac{\hat{\delta}(s)}{\hat{P}_o(s)} = \frac{\frac{1}{J\omega_n}}{s\left(s + \frac{k_p + D\omega_n}{J\omega_n}\right)} = \frac{b_p}{s\,(s+a_p)}, \tag{29}$$

where $b_p = 1/J\omega_n$, and $a_p = (k_p + D\omega_n)/J\omega_n$ are the controller gains. Thus, considering the active power model described by (17) the open-loop transfer function for VSG active power control is given as:

$$T_P(s) = \frac{b_p h_p}{s\,(s+a_p)\left(s^2 + \frac{2R_g}{L_g}s + \frac{R_g^2 + (\omega_g L_g)^2}{L_g^2}\right)}, \tag{30}$$

where it was assumed that the voltage and current controllers are significantly faster than the VSG power flow controllers, and hence its dynamics can be neglected in the power control loop to reduce design complexity. The design criterion applied to active power controller must determine three parameters which are the droop coefficient k_p, inertia moment J and damping factor D. The droop coefficient k_p is determined based on the Grid Codes Recommendations (EN 50438, 2015). Based on this recommendation, it is required that a change of 100% in active power must correspond to a change of 2% in grid frequency. Therefore, for the grid-tied converter power rating (see Table 1), the droop coefficient is calculated as:

$$k_p = \frac{\Delta P_{max}}{\Delta\omega_{max}} = \frac{10000}{(2\pi 60) \times 0.02} = 1326.3\ (W.s/rad). \tag{31}$$

The performance requirements applied for determining the swing equation gains employ $\%OS = 10\%$ and $T_{s2\%} = 0.5$ s, i.e., $\xi_p = 0.6$ and $\omega_p = 13.4$ rad/s. Thus, the desired dominant closed-loop pole can be calculated as:

$$s_d = -\xi_p\omega_p + j\omega_p\sqrt{1-\xi_p^2} = -8 + j10.68. \tag{32}$$

Based on the design criteria employed in RLM, the angular contribution required from the controller pole is calculated for satisfy the following angle restriction:

$$\angle T_P(s_d) = -180\,^\circ. \tag{33}$$

Then, the controller gain can be calculated by the module restriction, which addresses the following expression:

$$b_p = \frac{1}{|T_P(s_d)|}. \tag{34}$$

Therefore, considering the required performance for active power controller and system parameters given by Table 1, the controller gains are determined by substitution of these parameters into (33) and (34), which results in $a_p = 16.26$ and $b_p = 7.28 \times 10^{-3}$, or $J = 0.3644$ and $D = 2.4067$. Fig. 6(a) shows the resulting root locus for VSG active power control loop. The closed-loop system has two complex dominant poles, which corresponds to the desired pole s_d, and two complex non-dominant poles furthest to the origin. The X/R ratio variation effect in the location of the system closed-loop poles are presented in Fig. 6(b). As X/R ratio increases, the complex non-dominant poles are closer to the imaginary axis, which corresponds to increases its contribution in the system dynamic response. On the other hand, the complex dominant poles are closer to the real axis, which results in a more dampened transient response. Therefore, the X/R ratio variation affects the designed controller dynamic performance.

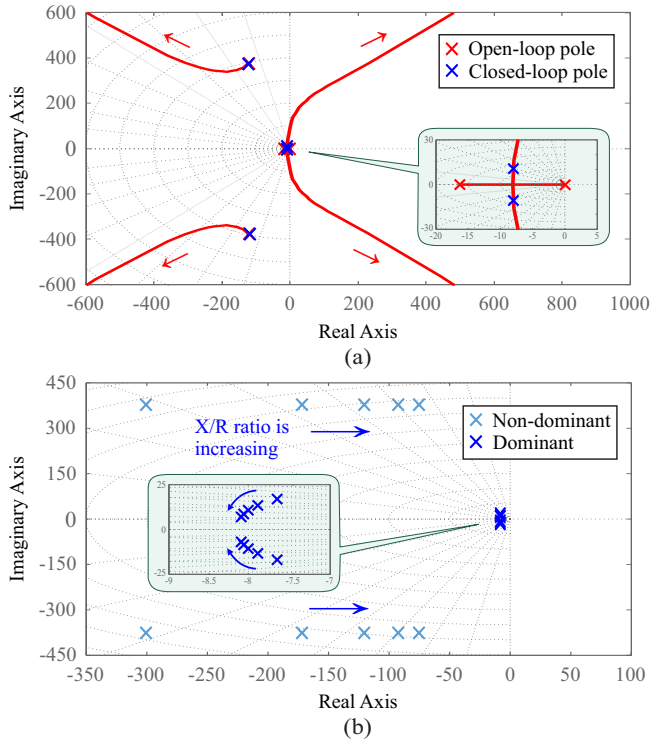

Figure 6. VSG active power control loop (a) Root locus (b) Closed-loop poles when X/R ratio varies.

VSG Reactive Power Controller. From the block diagram of Fig. 1 and considering $\sqrt{3}V_o \approx v_{od}^{e*}$, the controller transfer function that regulate the VSG reactive power can be given by:

$$R_Q(s) = \frac{\hat{V}_o(s)}{\hat{Q}_o(s)} = \frac{K}{s + Kk_q}. \tag{35}$$

Thus, considering the reactive power model described by (20) the open-loop transfer function for VSG reactive power control is expressed as:

$$T_Q(s) = \frac{Kh_q}{(s + Kk_q)\left(s^2 + \frac{2R_g}{L_g}s + \frac{R_g^2 + (\omega_g L_g)^2}{L_g^2}\right)}. \tag{36}$$

The design criterion applied to reactive power controller must determine two parameters which are the droop coefficient k_q, and integral coefficient K. Assuming a similar procedure to the used for active power controller, the droop coefficient k_q is determined based on the Grid Codes Recommendations (EN 50438, 2015), in which a change of 100% in reactive power must correspond to a change of 10% in grid voltage. Therefore, for the grid-tied converter power rating (see Table 1), the droop coefficient is calculated as:

$$k_q = \frac{\Delta Q_{max}}{\Delta V_{max}} = \frac{10000}{127\sqrt{2} \times 0.1} = 556.78\ (A). \tag{37}$$

The performance requirement used for determining the controller gains employs $T_{s2\%} = 0.4\ s$, which corresponds to the following desired dominant closed-loop pole $s_d = -10$. Therefore, the controller gain that address this design requirement is calculated as $K = 0.0538$. Fig. 7(a) shows the resulting root locus for VSG reactive power control loop. The closed-loop system has one real dominant poles, which corresponds to the desired pole s_d, and two complex non-dominant poles furthest to the origin. Fig. 7(b) shows the effect of the X/R ratio variation in the system closed-loop poles. With increasing X/R ratio the complex non-dominant poles are closer to the imaginary axis, while the real dominant pole are closer to the origin, which results in a more slow transient response. Therefore, the X/R ratio variation affect compensated system dynamic performance.

4. SIMULATION RESULTS

For evaluating the effectiveness of the small-signal models and the parameter design applied to the VSG control loops the system topology presented in Fig. 1 is implemented in PSIM. The simulation study employs the same parameters of those listed in Table 1.

4.1 VSG Controllers Performance Analysis

Fig. 8 shows the VSG controllers dynamic performance when it is added an active power step variation between 0 and 10 kW, while reactive power is set in 0. According to Fig. 8(a), the active power converges to its reference value accurately. Besides, its transient response presents $\%OS$ and settling time approximately equal to 9.2% and 0.45 s, respectively. According to Fig. 8(b), the PCC voltages converge to its reference values accurately with $\%OS$ and settling time approximately equal to 16% and 1.4 ms, respectively. According to Fig. 8(c), the VSI output currents converge fast to its reference values with settling time approximately equal to 1.2 ms. Therefore, these results demonstrate the effectiveness of VSG controllers for this operating scenario.

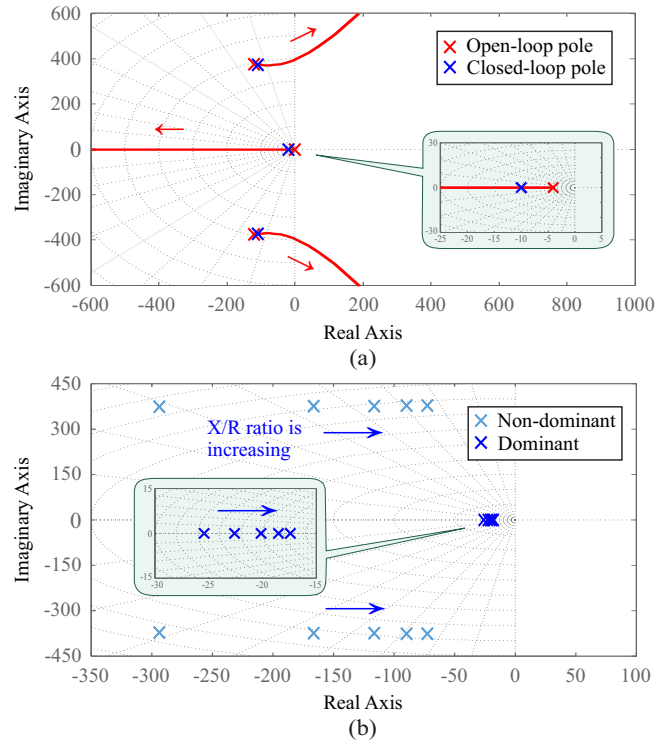

Figure 7. VSG reactive power control loop (a) Root locus (b) Closed-loop poles when X/R ratio varies.

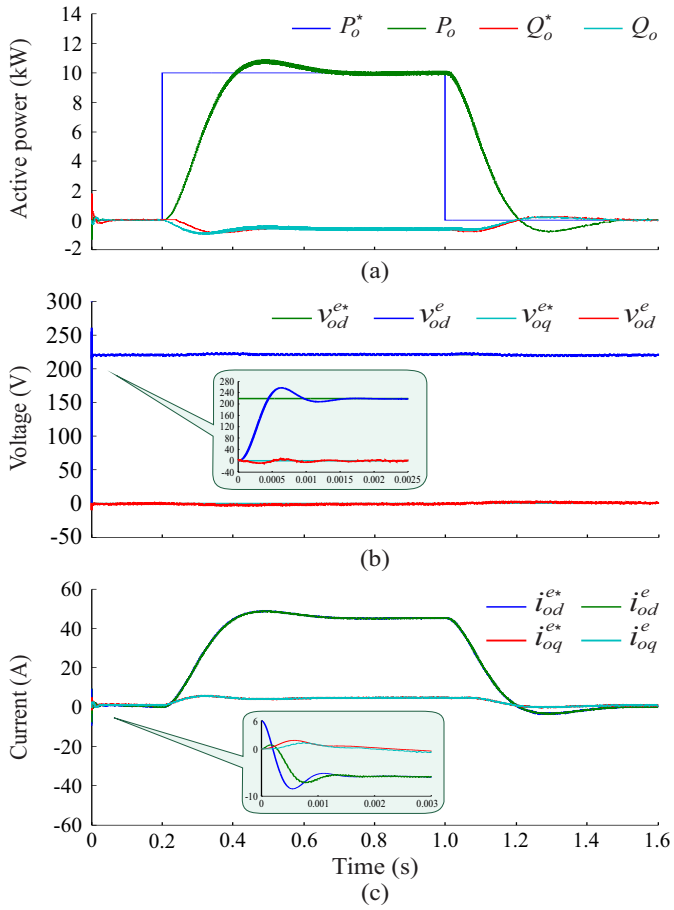

Figure 8. Simulation Results for the controlled (a) Active power (b) PCC voltages (c) VSI output currents.

Fig. 9 presents the VSG controller dynamic performance during reactive power step variation between 0 and 10 kvar, while active power is set in 0. Based on Fig. 9(a), the reactive power converges to its reference value accurately with a settling time of approximately 0.36 s. Figs. 9(b) and (c) present the PCC voltages and VSI output currents. Voltage and current controllers have dynamic performance similar to the previous operating scenario. These results again prove the effectiveness of VSG controllers.

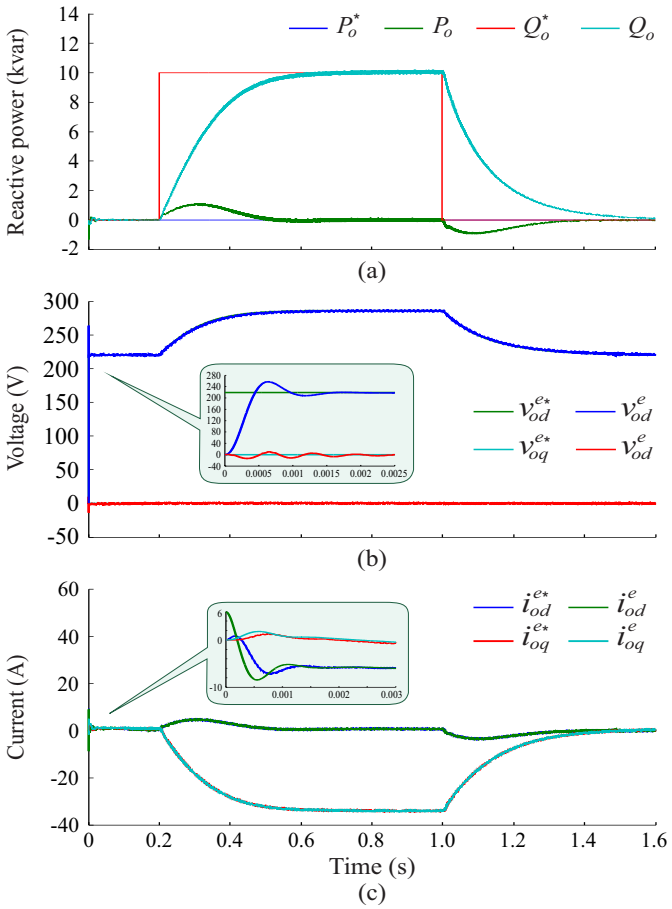

Figure 9. Simulation Results for the controlled (a) Reactive power (b) PCC voltages (c) VSI output currents.

4.2 Performance Analysis for Line Impedance Variation

Figs. 10(a) and (b) present the VSG active and reactive power dynamic behavior under the X/R ratio variation effect considering an P_o^* step variation between 0 and 10 kW, while $Q_o^* = 0$ and Q_o^* step variation between 0 and 10 kvar, while $P_o^* = 0$, respectively. The active and reactive power converge to their reference values. Besides, for 10% variations in X/R ratio their transient responses yet present $\%OS$ and settling time suitable values. However, 50% variations in X/R ratio significantly modified the system dynamic performance. For $0.5X/R$ dynamic responses were more oscillatory, while $1.5X/R$ resulted in more dampened dynamic responses with longer rising times. Therefore, as discussed in Sections II and III, a much high variation in the X/R ratio can result in the degradation of the system dynamic performance.

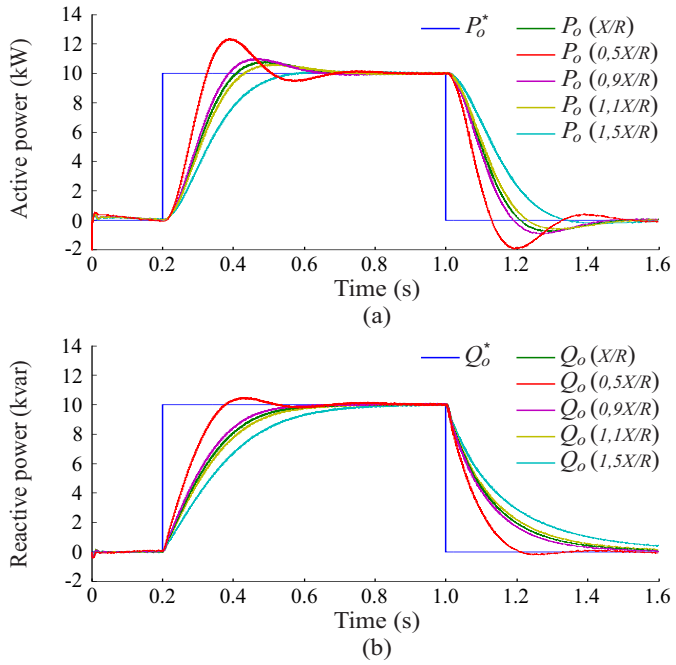

Figure 10. Power regulation with variation of X/R ratio. (a) Active power (b) Reactive power.

5. CONCLUSIONS

This paper presented a grid-tied distributed generation system implementation that uses the virtual synchronous generator approach in order to realize support for grid frequency and voltage. The small-signal modeling of system control loops was described, and its dynamic characteristics analyzed. The design criteria applied to controllers was presented, and the control parameters determined. Besides, the line impedance influence on the power flow dynamic behavior was discussed, and its effect presented. Simulation results demonstrate the effectiveness of the theoretical analysis and parameters design method. However, the large the line impedance variations from design parameters the large the control performance degradation, what will be treated in a future works.

ACKNOWLEDGMENT

The authors would like to thank the CAPES (Coordenação de Aperfeiçoamenteo de Pessoal de Nível Superior) and CNPq (Conselho Nacional de Pesquisa).

REFERENCES

Akagi, H., Watanabe, E.H., and Aredes, M. (2017). *Instantaneous Power Theory and Applications to Power Conditioning*. John Wiley & Sons, Ltd, Piscataway, NJ, USA, 2nd edition.

Azmy, A.M. and Erlich, I. (2005). Impact of distributed generation on the stability of electrical power system. In *IEEE Power Engineering Society General Meeting, 2005*, 1056–1063 Vol. 2.

Blaabjerg, F., Teodorescu, R., Liserre, M., and Timbus, A.V. (2006). Overview of control and grid synchronization for distributed power generation systems. *IEEE Transactions on Industrial Electronics*, 53(5), 1398–1409.

Blasko, V. (1996). Analysis of a hybrid pwm based on modified space vector and triangle comparison methods. In *IAS '96. Conference Record of the 1996 IEEE Industry Applications Conference Thirty-First IAS Annual Meeting*, volume 2, 947–955 vol.2.

Du, Y., Guerrero, J.M., Chang, L., Su, J., and Mao, M. (2013). Modeling, analysis, and design of a frequency-droop-based virtual synchronous generator for microgrid applications. In *2013 IEEE ECCE Asia Downunder*, 643–649.

EN 50438 (2015). Requirements for the connection of micro-generators in parallel with public low-voltage distribution networks. *CEI EN 50438*, 1–12.

Guerrero, J.M., de Vicuna, L.G., Matas, J., Castilla, M., and Miret, J. (2004). A wireless controller to enhance dynamic performance of parallel inverters in distributed generation systems. *IEEE Transactions on Power Electronics*, 19(5), 1205–1213.

Guerrero, J.M., Matas, J., Garcia de Vicuna, L., Castilla, M., and Miret, J. (2007). Decentralized control for parallel operation of distributed generation inverters using resistive output impedance. *IEEE Transactions on Industrial Electronics*, 54(2), 994–1004.

Mo, O., D'Arco, S., and Suul, J.A. (2017). Evaluation of virtual synchronous machines with dynamic or quasi-stationary machine models. *IEEE Transactions on Industrial Electronics*, 64(7), 5952–5962.

Rocabert, J., Luna, A., Blaabjerg, F., and Rodríguez, P. (2012). Control of power converters in ac microgrids. *IEEE Transactions on Power Electronics*, 27(11), 4734–4749.

Shuai, Z., Sun, Y., Shen, Z., Tian, W., Tu, C., Li, Y., and Yin, X. (2016). Microgrid stability: Classification and a review. *Renewable and Sustainable Energy Reviews*, 58, 167–179.

Song, Z., Zhang, J., Tang, F., Wu, M., Lv, Z., Sun, L., and Zhao, T. (2018). Small signal modeling and parameter design of virtual synchronous generator to weak grid. In *2018 13th IEEE Conference on Industrial Electronics and Applications (ICIEA)*, 2618–2624.

Wu, H., Ruan, X., Yang, D., Chen, X., Zhao, W., Lv, Z., and Zhong, Q. (2016). Small-signal modeling and parameters design for virtual synchronous generators. *IEEE Transactions on Industrial Electronics*, 63(7), 4292–4303.

Zhang, L., Harnefors, L., and Nee, H. (2010). Power-synchronization control of grid-connected voltage-source converters. *IEEE Transactions on Power Systems*, 25(2), 809–820.

Zhong, Q. (2016). Virtual synchronous machines: A unified interface for grid integration. *IEEE Power Electronics Magazine*, 3(4), 18–27.